Protein Engineering, Design & Selection vol. 24 no. 7 pp. 553–563, 2011
Published online April 25, 2011 doi:10.1093/protein/gzr018

The induction of α-helical structure in partially unfolded HypF-N does not affect its aggregation propensity

B.Ahmad[1,4], I.Vigliotta[1], F.Tatini[1], S.Campioni[1,5], B.Mannini[1], J.Winkelmann[1,6], B.Tiribilli[2] and F.Chiti[1,3,7]

[1]Dipartimento di Scienze Biochimiche, Università degli Studi di Firenze, Viale Morgagni 50, 50134, Firenze, Italy, [2]Consiglio Nazionale delle Ricerche (CNR), Istituto dei Sistemi Complessi, Via Madonna del Piano 10, 50019 Sesto Fiorentino, Firenze, Italy, [3]Consorzio Interuniversitario, Istituto Nazionale Biostrutture e Biosistemi (I.N.B.B.), Viale delle Medaglie d'Oro 305, 00136 Roma, Italy, [4]Present address: Department of Physics and Astronomy, Michigan State University, East Lansing, Michigan 48824, USA, [5]Present address: Department of Chemistry and Applied Biosciences, Laboratory of Physical Chemistry, Eidgenössische Technische Hochschule Zürich, Wolfgang Pauli Str. 10, 8093 Zurich, Switzerland and [6]Present address: Magnetic Resonance Center (CERM), University of Florence, Via Luigi Sacconi 6, 50019 Sesto Fiorentino, Firenze, Italy
[7]To whom correspondence should be addressed. Email: fabrizio.chiti@unifi.it

Received March 18, 2011; revised March 29, 2011; accepted March 29, 2011

Edited by Daniel Otzen.

The conversion of proteins into structured fibrillar aggregates is a central problem in protein chemistry, biotechnology, biology and medicine. It is generally accepted that aggregation takes place from partially structured states of proteins. However, the role of the residual structure present in such conformational states is not yet understood. In particular, it is not yet clear as to whether the α-helical structure represents a productive or counteracting structural element for protein aggregation. We have addressed this issue by studying the aggregation of pH-unfolded HypF-N. It has previously been shown that the two native α-helices of HypF-N retain a partial α-helical structure in the pH-unfolded state and that these regions are also involved in the formation of the cross-β structure of the aggregates. We have introduced mutations in such stretches of the sequence, with the aim of increasing the α-helical structure in the key regions of the pH-unfolded state, while minimizing the changes of other factors known to influence protein aggregation, such as hydrophobicity, β-Sheet propensity, etc. The resulting HypF-N mutants have higher contents of α-helical structure at the site(s) of mutation in their pH-unfolded states, but such an increase does not correlate with a change of aggregation rate. The results suggest that stabilisation of α-helical structure in amyloidogenic regions of the sequence of highly dynamic states does not have remarkable effects on the rate of protein aggregation from such conformational states. Comparison with other protein systems indicate that the effect of increasing α-helical propensity can vary if the stabilised helices are in non-amyloidogenic stretches of initially unstructured peptides (accelerating effect), in amyloidogenic stretches of initially unstructured peptides (no effect) or in amyloidogenic stretches of initially stable helices (decelerating effect).

Keywords: aggregation mechanism/amyloid fibrils/on-pathway/protein misfolding/α-helical intermediate

Introduction

Proteins and peptides have a generic propensity to form well-organised fibrillar aggregates characterised by an extended cross-β structure, generally referred to as amyloid-like fibrils (Dobson, 1999; Dobson and Stefani, 2003; Uversky and Fink, 2004; Chiti and Dobson, 2006). From a physicochemical perspective, this process represents an essential feature of the behaviour of polypeptide chains that needs to be fully understood for a thorough characterisation of the nature of proteins (Jahn and Radford, 2008). From a more biological perspective, formation of amyloid fibrils, or intracellular inclusions with structurally related characteristics, is associated with a large number of pathological conditions in humans (Chiti and Dobson, 2006). It is also a major problem in biotechnology as the large-scale expression of proteins potentially interesting to the market often results in their self-assembly in inclusion bodies with amyloid-like structural features (Ventura and Villaverde, 2006).

It is well accepted that the process of amyloid fibril formation by normally globular proteins requires a partial or global unfolding of the native structure across the major free-energy barrier for unfolding or, alternatively, structural and transient fluctuations from the native state ensemble (Chiti and Dobson, 2009). Several studies have shown that aggregation of highly flexible, partially folded states is promoted by regions of the sequence with a high hydrophobicity and high propensity to form β-sheet structure, resulting in mathematical algorithms able to predict the aggregation-promoting regions in a protein from the knowledge of its sequence (Fernandez-Escamilla *et al*., 2004; Yoon and Welsh, 2004; Pawar *et al*., 2005; Tartaglia *et al*., 2005; Trovato *et al*., 2006; Galzitskaya *et al*., 2006; Conchillo-Solé *et al*., 2007; Maurer-Stroh *et al*., 2010). It is not clear, however, if the residual structure present in the aggregation-competent state plays an important role in the process. While it is widely recognised that an efficient mechanism to neutralise the amyloidogenic potential of aggregation-promoting regions is to promote their folding into a stable and persistent structure, such as that of the native state of a globular protein (Dobson, 1999; Uversky and Fink, 2004; Monsellier and Chiti, 2007; Tzotzos and Doig, 2010), it is still unclear as to whether the flexible structure present in partially folded states of proteins plays a role in the process of aggregation from such states. Similarly, it is not clear as to whether the formation of structure in intrinsically disordered proteins plays a role in the process of amyloid formation by such systems.

In particular, the results describing the role of α-helical structure are contradictory. The formation of amyloid fibrils by the 40- and 42-residue forms of the amyloid β (Aβ) peptide has been shown to be preceded by the formation of oligomeric species with α-helical structure, leading to the conclusion that an α-helical containing oligomer is an on-pathway species necessary to form fibrils (Kirkitadze *et al*., 2001). Such a hypothesis was reinforced by the finding that small-to-moderate concentrations of the α-helical inducer 2,2,2-trifluoroethanol (TFE) is able to shorten the lag phase of amyloid fibril formation by the Aβ peptide (Fezoui and Teplow, 2002). Another widely studied intrinsically disordered peptide, namely the islet amyloid polypeptide (IAPP), was shown to form transiently α-helical structure and aggregate more rapidly in the presence of model phospholipid membranes (Knight *et al*., 2006; Ling *et al*., 2009). Fibril formation by IAPP was also found to be accelerated in the presence of small concentrations of hexafluoroisopropanol (Padrick and Miranker, 2002; Abedini and Raleigh, 2005). In contrast to these findings, other reports have shown that the increase in the α-helical propensity of specific regions of the sequence by protein engineering results in a significant deceleration of the process of amyloid fibril formation (Villegas *et al*., 2000; Päiviö *et al*., 2004).

None of such studies can, however, directly address this issue: in the absence of appropriate kinetic tests, the early appearance of oligomers with α-helical structure is not a direct demonstration that the oligomers are on-pathway and that the α-helical structure contained in such oligomers is a productive type of structure for the formation of the fibrils (Abedini and Raleigh, 2009). The addition of TFE causes dramatic changes to the property of the solution, modifies the dynamics of the polypeptide chain and stabilises hydrogen bonds more generally (not only those of the α-helical structure, but also those of the cross-β structure of the fibrils). It is thus difficult to correlate the TFE-induced acceleration of aggregation to the requirement of forming α-helical structure during aggregation. On the other hand, mutations used to stabilise the α-helical structure often involve dramatic changes of the hydrophobicity, β-sheet propensity and charge of the sequence at the site of mutation. Since such factors are demonstrated to be important determinants of the aggregation rate of an unstructured polypeptide chain, changes of the aggregation rate resulting from such mutations cannot be attributed unambiguously to the induced changes of the α-helical structure.

In this work we have attempted to circumvent the problem using the N-terminal domain of the *Escherichia coli* protein HypF (HypF-N). This protein domain folds with a well-characterised mechanism (Calloni *et al*., 2003) and was shown to form amyloid-like fibrils structurally, morphologically and tinctorially indistinguishable from those associated with disease (Chiti *et al*., 2001; Relini *et al*., 2004; Marcon *et al*., 2005). It was also shown to form amyloid-like protofibrils positive to thioflavin T (ThT) and containing β-sheet at pH values lower than 2.3 and at ionic strength values higher than 100 mM (Campioni *et al*., 2008; Calloni *et al*., 2008; Campioni *et al*., 2010). Under such conditions of low pH HypF-N retains, in the acid-unfolded, monomeric state populated before aggregation, a partially folded conformation, where the two regions of the sequence adopting α-helical structure in the native state (residues 22–32 and 55–63) are not completely unfolded, as monitored with far-UV circular dichroism (CD) and nuclear magnetic resonance (NMR) (Campioni *et al*., 2008; Calloni *et al*., 2008). Importantly, both regions of the sequence have been shown to play an important role in the process of amyloid-like protofibril formation, as deduced from the ability of mutations located in these two regions to significantly affect such a process (Calloni *et al*., 2008). In addition, structural information indicates that such regions form the structural core of the resulting aggregates, meaning that most, if not all, of their residues form the β-sheet structure stabilising the aggregates (Campioni *et al*., 2010). These findings make HypF-N an ideal system to explore the role of α-helical structure in the process of amyloid fibril formation. Indeed, the regions of the sequence adopting an α-helical conformation in the native state (residues 22−32 and 55−63) not just partially retain α-helical structure in the partially folded acid-denatured state, but are also involved in the process of aggregation of such a conformational state into amyloid-like protofibrils, thus encouraging an investigation of the importance of the α-helical structure in the process of aggregation.

For this purpose, we have introduced specific mutations that increase significantly the α-helical propensity of these two regions of the sequence, while minimising the changes of the other factors affecting aggregation and, as a consequence, minimising the changes to the intrinsic (sequence-based) propensity to form amyloid fibrils of the acid-denatured state. We will show that the resulting HypF-N variants are characterised by a higher amount of α-helical structure at the sites of mutation in the acid-unfolded state, but aggregate with a rate similar to that of the wild-type protein, ruling out that formation or stabilisation of α-helical structure in a highly dynamic state has a fundamental role in the process of amyloid formation.

Materials and methods

HypF-N mutants production, expression and purification

All the HypF-N mutants were produced using the QuikChange site-directed mutagenesis kit (Stratagene, La Jolla, CA, USA) and DNA sequencing was used to ensure the presence of the desired mutation(s). The genes for wild-type and mutant HypF-N were cloned in a modified pQE30-Xa plasmid (Qiagen S.p.A, Milano, Italy), in which the DNA stretch coding for the factor Xa cleavage site was changed into a sequence coding for the thrombin cleavage site (pQE30-Th) (Campioni *et al*., 2008). The protein was expressed in *E. coli* XL1-Blue cells transformed with the pQE30-Th plasmid and purified as described previously (Campioni *et al*., 2008). Protein purity was assessed by SDS-PAGE and was found to be >95%. Protein concentration was assessed by optical absorption ($\epsilon_{280} = 12{,}490$ $M^{-1}\,cm^{-1}$) and stock solutions were stored at −20°C in 5 mM acetate, 2 mM dithiothreitol (DTT), pH 5.5.

Acid-induced unfolding of HypF-N mutants

Buffer solutions were prepared at various pH values ranging from 7.0 to 1.0. For pH values of 5.7–7.0, 3.9–5.1 and 2.1–3.7, solutions containing 25 mM 3,3-dimethylglutarate, 50 mM acetate and 50 mM citrate were used, respectively. pH values <2.0 were obtained by adding different amounts

of trifluoroacetic acid (TFA). Since a given compound can buffer the pH only in a limited range of pH ($pK_a-1 < pH < pK_a+1$), it was necessary to use different compounds to cover the pH range under investigation (1.0–7.0). All solutions contained 2 mM β-Mercaptoethanol to maintain the three cysteine residues in a reduced form, and a total ionic strength of 50 mM was achieved for all solutions by adding different amounts of NaCl. The samples containing 19 and 1.9 μM protein were then subjected to far-UV CD and intrinsic fluorescence analyses, respectively. For this purpose, a Jasco J-810 spectropolarimeter (Tokyo, Japan) equipped with a thermostated cell holder attached to a Thermo Haake C25P water bath (Karlsruhe, Germany) and a Perkin-Elmer LS 55 spectrofluorimeter (Wellesley, MA, USA) equipped with a thermostated cell holder attached to a Haake F8 water bath (Karlsruhe, Germany) were used, respectively. Plots of wavelength of maximum fluorescence emission (λ_{max}) and mean residue ellipticity at 222 nm ($[\theta]_{222}$) were fitted to a sigmoidal function of the form:

$$y = (q_1 + m_1 \cdot \mathrm{pH}) + (q_2 + m_2 \cdot \mathrm{pH}) \cdot \{10^{n(\mathrm{pH}-\mathrm{p}Ka)}/[1 + 10^{n(\mathrm{pH}-\mathrm{p}Ka)}]\} \quad (1)$$

where q_1, q_2, m_1 and m_2 are the intercept (q) and angular coefficient (m) values of the post- and pre-transition baselines, respectively; n is the number of protons involved in the transition; p*K*a refers to the p*K*a value(s) of the residues titrated in the transition. m_1 and m_2 values were constrained to 0 in our analysis.

Urea-induced unfolding of HypF-N mutants

For each HypF-N variant, 18 samples containing 19 μM HypF-N, 25 mM 3,3-dimethylglutarate, 2 mM DTT, pH 7.0 and different concentrations of urea, ranging from 0 to 8.0 M, were prepared. Other 18 samples containing 19 μM HypF-N, 20 mM TFA, 30 mM NaCl, 2 mM DTT, pH 1.7 and different concentrations of urea, ranging from 0 to 8.0 M, were prepared. All samples were equilibrated for 2 h at 25°C and subjected to far-UV CD analysis. The unfolding parameters ΔG^{H_2O} and m, were obtained from plots of $[\theta]_{222}$ versus urea concentration by a non-linear regression analysis of the data using the following equation (Santoro and Bolen, 1988):

$$[\theta]_{222} = [(Y_N + m_N[\mathrm{urea}]) + (Y_U + m_U[\mathrm{urea}]) \cdot \exp(-\Delta G^{H_2O} + m[\mathrm{urea}])/RT]/[1 + \exp(-\Delta G^{H_2O} + m[\mathrm{urea}])/RT] \quad (2)$$

where $[\theta]_{222}$ is the mean residue ellipticity, Y_N and Y_U represent the intercepts and m_N and m_U the slopes of the pre-transition (native protein) and post-transition (unfolded protein) baselines, respectively. Thus, fits of urea-induced equilibrium unfolding data to equation (2) yield values for ΔG^{H_2O} and m. ΔG^{H_2O} is the standard free-energy changes for the unfolding transition in the absence of denaturant, and m is the denaturant susceptibility parameter that describes the dependence of ΔG^{H_2O} on denaturant concentration. The ratio between the ΔG^{H_2O} and m values provides the mid-point of urea-induced unfolding (C_m).

Far-UV CD

Far-UV CD spectra were acquired at 25°C for all the HypF-N variants using solutions containing 19 μM protein, 20 mM TFA, 30 mM NaCl, 2 mM DTT, pH 1.7. A 1-mm path-length cell and a Jasco J-810 spectropolarimeter (Tokyo, Japan) equipped with a thermostated cell holder attached to a Thermo Haake C25P water bath (Karlsruhe, Germany) were used. The α-helical content was estimated from the mean residue ellipticity at 222 ($[\theta]_{222}$) following the equation (Morrow *et al*., 2002):

$$\%\,\alpha - \mathrm{helix} = (-[\theta]_{222} + 3000)/39000 \quad (3)$$

The increase in percent α-helical content at the site of mutation (I-α_{MUT}) was obtained using:

$$I\text{-}\alpha_{MUT} = [(\%\,\alpha - \mathrm{helix})_{MUT} - (\%\,\alpha - \mathrm{helix})_{WT}] \times N_\alpha/N_{TOT} \quad (4)$$

where $(\%\ \alpha\text{-helix})_{MUT}$ and $(\%\ \alpha\text{-helix})_{WT}$ are the percentages of α-helical structure of the overall mutated and wild-type sequences, respectively; N_α and N_{TOT} are the number of residues in the mutated helix and overall sequence, respectively. According to this scale, a I-α_{MUT} value of 25% does not mean that the α-helical content of the mutated helix has increased by 25% relative to the wild-type helix, but that the α-helical content of the mutated helix has increased by 25% in a scale from 0 (no helix) to 100% (fully formed helix), independently of the initial value of the wild-type helix.

Intrinsic fluorescence

All samples, initially containing 19 μM HypF-N, 20 mM TFA, 30 mM NaCl, 2 mM DTT and pH 1.7 were diluted 10-fold in the same solution conditions immediately before the measurements. Final protein concentration was 1.9 μM. Intrinsic fluorescence emission spectra were acquired at 25°C from 300 to 400 nm with excitation at 280 nm. A Perkin-Elmer LS 55 spectrofluorimeter (Wellesley, MA, USA), equipped with a thermostated cell holder attached to a Haake F8 water bath (Karlsruhe, Germany), and a 2-mm × 10-mm path-length quartz cell, were used.

ANS fluorescence

ANS fluorescence spectra were acquired at 25°C for all the HypF-N variants using solutions containing 5 μM protein, 20 μM ANS, 20 mM TFA, 30 mM NaCl, 2 mM DTT and pH 1.7. 8-Anilinonaphthalene-1-sulphonate (ANS) was purchased from Sigma-Aldrich. Fluorescence spectra were acquired at 25°C immediately after dilution of the protein variants into the conditions of analysis. The same cell and equipment described above, with an excitation wavelength of 380 nm and an emission range from 400 to 600 nm, were used. A spectrum was also acquired in the absence of protein and subtracted from all the spectra acquired in the presence of protein. All the spectra are reported according to this subtraction procedure.

Dynamic light scattering

HypF-N and its variants were incubated for 30 min at a protein concentration of 38 μM in 20 mM TFA, 30 mM NaCl, 2 mM DTT and pH 1.7. In each case the protein stock

solution was filtered with a 20-nm syringe filter (Whatman, Maidstone, UK) immediately before sample preparation. Buffer solutions were also filtered. The dynamic light-scattering (DLS) measurements were performed at 25°C using the Malvern Zetasizer Nano S instrument (Malvern, Worcestershire, UK), equipped with a Peltier temperature controller. Disposable polystyrene cuvettes having a 1-cm path length were used. Every sample was measured three times and the average distributions are reported. For each protein variant, the average and the standard error values of the sizes corresponding to the peak of interest in each of these three distributions were used as a measure of the apparent hydrodynamic diameter and associated experimental error, respectively.

ThT fluorescence

Aggregation of each HypF-N variant was initiated by incubating the protein, at a concentration of 48 μM, in 20 mM TFA, 330 mM NaCl, 2 mM DTT, pH 1.7, 25°C. At regular time interval aliquots of 60 μl were mixed with 440 μl of 25 mM phosphate buffer, pH 6.0, containing 25 μM ThT and the resulting fluorescence was measured using a Perkin-Elmer LS 55 spectrofluorimeter (Wellesley, MA, USA) equipped with a thermostated cell holder attached to a Haake F8 water bath (Karlsruhe, Germany) at excitation and emission wavelengths of 440 and 485 nm, respectively. A 2 × 10-mm path-length quartz cell was used. Plots of ThT fluorescence against time were fitted to a single exponential function:

$$F(t) = F^{\infty} + \Delta F \cdot \exp(-k_{agg}t) \quad (5)$$

where $F(t)$ represents the fluorescence as a function of time, ΔF is the amplitude of the observed change in ThT fluorescence, F^{∞} is the fluorescence at the plateau and k_{agg} is the aggregation rate constant. The analysis yielded the rate constant for aggregation (k_{agg}) for each HypF-N variant.

Atomic force microscopy

All HypF-N variants were incubated at a concentration of 48 μM for 2 h in 20 mM TFA, 330 mM NaCl, 2 mM DTT, pH 1.7, 25°C. Then 5 μL aliquots of 100-fold diluted samples were immediately deposited on a freshly cleaved mica substrate and dried under a gentle nitrogen flux. Non-contact AC mode atomic force microscopy (AFM) images were acquired in air using a PicoSPM microscope equipped with an AC-mode controller (Molecular Imaging, Phoenix, AZ). Rectangular non-contact cantilever (model NSG01, NT-MDT Moscow, Russia), with typical resonance frequency of 150 Khz, were used. Oligomer sizes were measured from the height in cross section of the topographic AFM images.

Results

Design of HypF-N variants with increased α-helical propensity at low pH

HypF-N contains two α-Helices in the native state, encompassing residues 22–32 and 55–63 (Fig. 1) (Rosano *et al.*, 2002). These two regions of the sequence were shown to maintain, at least partially, their α-helical conformation in the monomeric acid-unfolded state and were shown to play a relevant role in the conversion of acid-denatured HypF-N into oligomers with β-Sheet structure and ThT-binding (Calloni *et al.*, 2008; Campioni *et al.*, 2010). Mutations aimed at increasing the α-helical content of unfolded HypF-N at pH 1.7, without increasing its intrinsic aggregation propensity, were designed using the sequence-based AGADIR algorithm (Muñoz and Serrano, 1994) in conjunction with the ZYGGREGATOR (Tartaglia *et al.*, 2008), AGGRESCAN (Conchillo-Solé *et al.*, 2007) and PASTA (Trovato *et al.*, 2006) algorithms.

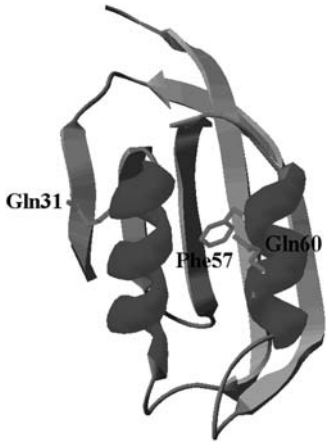

Fig. 1 Three-dimensional structure of native HypF-N (PDB ID 1GXU). The positions of the mutated residues are shown (Gln31, Phe57 and Gln60). These residues are all located in the two helices.

As shown by the α-helical propensity profiles generated by the AGADIR algorithm, the mutation Q31R, involving the first α-Helix, and the mutations Q60R and F57L/Q60R, involving the second α-Helix, are predicted to induce remarkable increases of the α-helical propensity at the corresponding sites of mutation (Fig. 2A). In contrast, all three mutations are predicted to cause very small changes, if any, of the aggregation propensity of the acid-unfolded state of HypF-N at the site of mutation, as shown by the analysis carried out with the ZYGGREGATOR (Fig. 2B), AGGRESCAN (Fig. 2C) and PASTA (Fig. 2D) algorithms. Similar results have been obtained using other algorithms able to predict, similarly to the three softwares shown here, the intrinsic aggregation propensity of a sequence from the sequence, without considering the influence of secondary and tertiary structure elements (Fernandez-Escamilla *et al.*, 2004; Yoon and Welsh, 2004; Tartaglia *et al.*, 2005; Galzitskaya *et al.*, 2006; Maurer-Stroh *et al.*, 2010; Chiti *et al.*, 2003). The selected mutations therefore represent valid probes of the effect of changing the level of residual α-helical structure in the regions of the sequence promoting aggregation from the acid-unfolded state of HypF-N without causing an increase of its intrinsic (sequence-based) aggregation propensity in the same regions. They will allow one to assess whether or not the stabilisation of the residual α-helical structure in the key regions of the acid-unfolded state causes an increase in the aggregation rate of the protein.

We have also considered mutations that decrease the α-helix content within the same two regions of the sequence 22–32 and 55–63. However, we considered this approach technically more difficult as mutations of this type would result also in a decrease of native state stability (i.e. in a

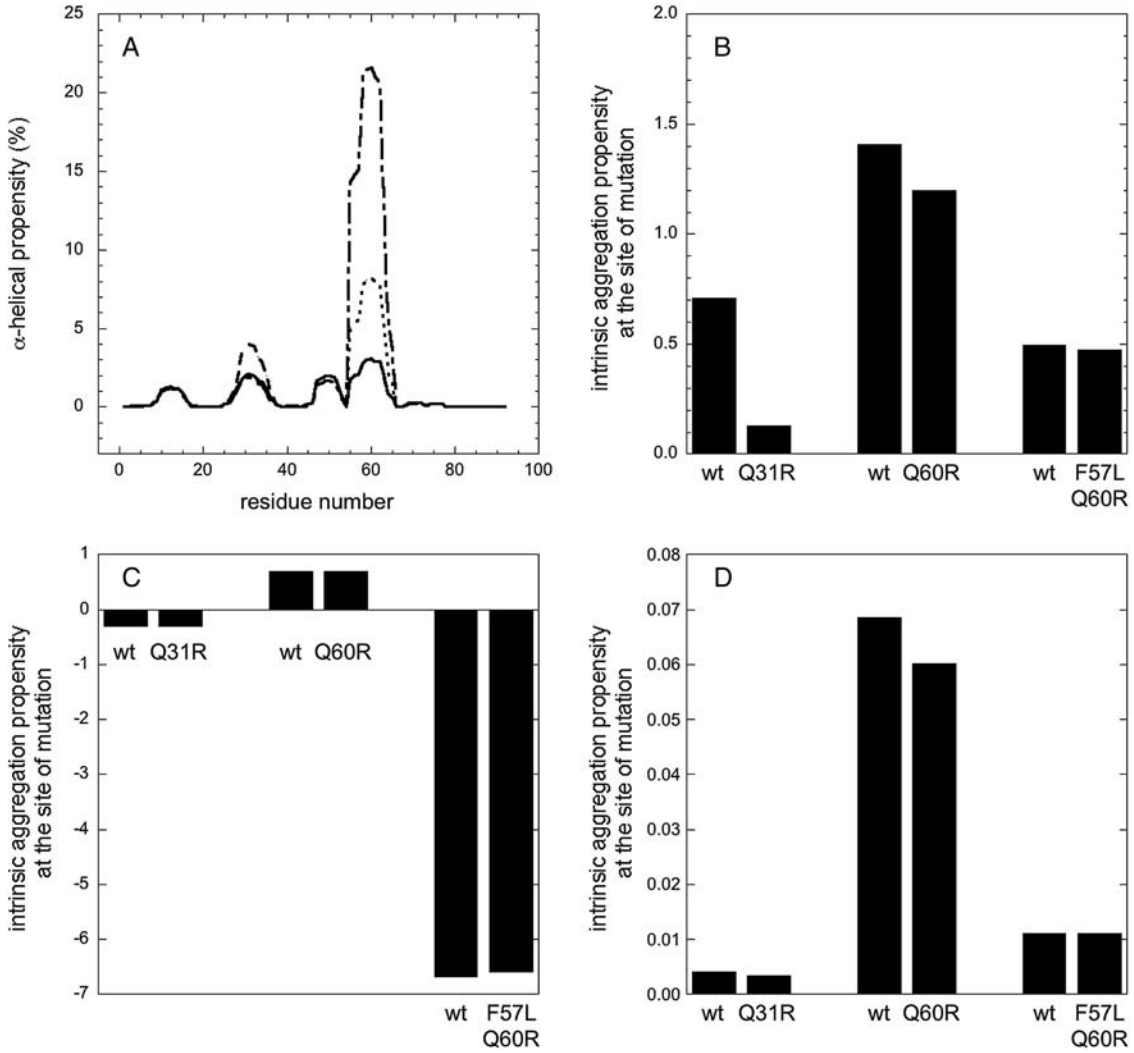

Fig. 2 (A) α-Helical propensity (%) along the HypF-N sequence calculated using the AGADIR algorithm for the wild-type (solid line), Q31R (dashed line), Q60R (dotted line) and F57L/Q60R (dotted-dashed line). (B–D) Intrinsic aggregation propensity of the various HypF-N mutants calculated at the site of mutation using the ZYGGREGATOR (B), AGGRESCAN (C) and PASTA (D) algorithms. Each graph reports the predictions of the three mutants at the site of mutation, beside the predictions of the wild-type sequence at the same site of mutation. When the algorithm required specific experimental conditions the calculations were carried out at 25°C, 50 mM ionic strength, pH 1.7.

decrease of $\Delta G_{F\text{-}U}$) and mutations of this type are known to result in HypF-N insolubility during purification (Calloni *et al*., 2005).

Acid-induced conformational transition of HypF-N variants

Acid-induced unfolding of wild-type and mutant HypF-N was followed by intrinsic fluorescence and far-UV CD spectroscopy as probes for tertiary and secondary structure of the protein, respectively (Fig. 3). Both optical probes show that wild-type and mutant HypF-N are conformationally stable from pH 7.0 to pH ~3.5, with a loss of both tertiary and secondary structure occurring in the 3.5–2.0 pH range. In all cases the unfolding transitions appear to be sharp and each pair of plots obtained with the same HypF-N variants and with the two probes are highly superimposable when normalised to the fraction folded (data not shown). The λ_{max} and $[\theta]_{222}$ data were fitted using a two-state transition model (equation (1)). The pK_a values of wild-type, Q31R, Q60R and F57L/Q60R HypF-N were calculated as 2.94 ± 0.06, 2.99 ± 0.06, 2.92 ± 0.06 and 2.86 ± 0.09, respectively, from λ_{max} data. The pK_a values were found to be 2.91 ± 0.03, 2.96 ± 0.03, 2.91 ± 0.05 and 2.90 ± 0.05, respectively, from $[\theta]_{222}$ data. For each HypF-N variant the pK_a values calculated from λ_{max} and $[\theta]_{222}$ data were very similar. Overall, the sharpness of the transitions, the good fitting of the two state model to the experimental data and the finding that each pair of the acid-unfolded curves give superimposable plots and identical midpoints, within experimental error, indicate that all the HypF-N variants studied here unfold at low pH via an apparent two-state mechanism.

This analysis also shows that none of the mutants is stabilised towards acid unfolding. However, the λ_{max} and $[\theta]_{222}$ of all the acid-unfolded mutants in the post-transition regions (i.e. at pH < 2.3) indicate the presence of higher levels of secondary and tertiary structure, compared to the acid-unfolded wild-type protein (Fig. 3A, B).

Conformational properties of HypF-N variants

In order to assess the secondary structure, tertiary structure, exposure of hydrophobic clusters and compactness of the HypF-N mutants in their acid-unfolded state relative to wild-type protein, all the HypF-N variants were subjected to

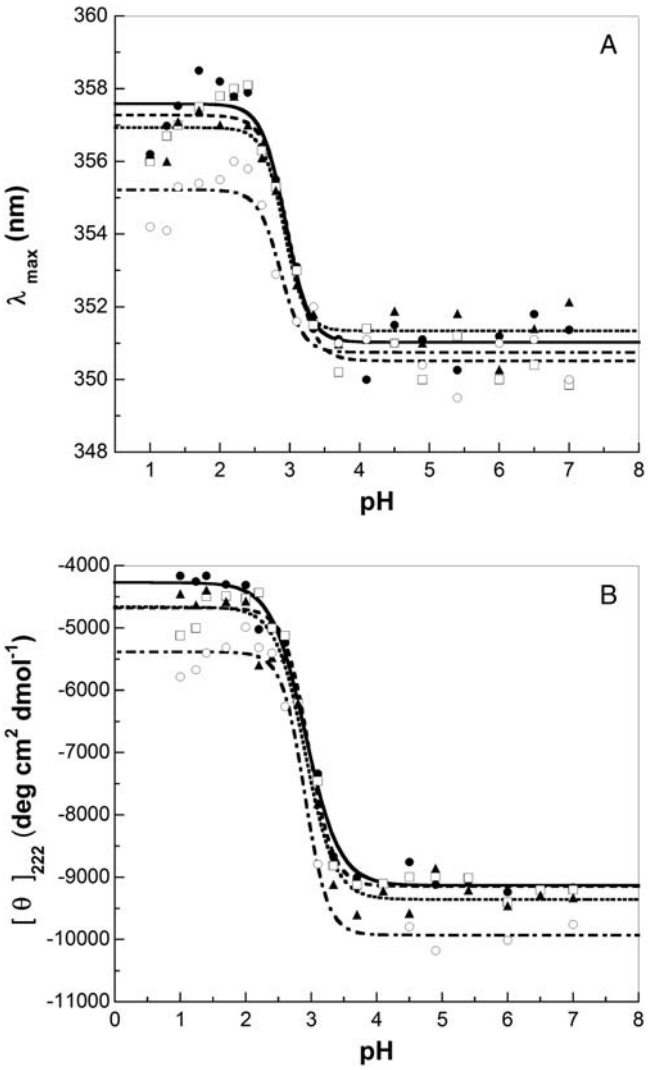

Fig. 3 Acid-induced unfolding at equilibrium of HypF-N variants monitored by (A) the wavelength of maximum fluorescence emission (λ_{max}) and (B) mean residue ellipticity at 222 nm ($[\theta]_{222}$). Data and lines of the best fit refer to wild-type (—•—), Q31R (–-□–-), Q60R (···▲···) and F57L/Q60R (–·–○–·–) HypF-N. The lines were obtained by fitting the data to a two-state model (equation (1)). Conditions were 50 mM total ionic strength, 2 mM DTT, 25°C.

far-UV CD, intrinsic fluorescence, ANS fluorescence and DLS measurements (Fig. 4). The far-UV CD spectrum of wild-type HypF-N at pH 1.7 has a strong negative signal at 201 nm, with a negative shoulder at 220–235 nm, showing that the protein retains elements of secondary structure at low pH (Fig. 4A). The spectrum is consistent with that previously observed under the same conditions of pH, ionic strength and temperature (Campioni *et al.*, 2008; Calloni *et al.*, 2008). The far-UV CD spectra of the Q31R, Q60R and F57L/Q60R mutants showed a negative CD band at 201, 203 and 206 nm, respectively (Fig. 4A). The red shift of the band was also found to correspond to a more marked negative signal at 220–235 nm, with the F57L/Q60R mutant exhibiting the most marked increment (Fig. 4A). These observations suggest an increased amount of secondary structure in the acid-unfolded mutants compared to wild-type HypF-N. The values of the total α-helical content in the acid unfolded states of the various mutants, as estimated from the $[\theta]_{222}$ values (equation (3)), are 10.52 ± 0.27, 10.90 ± 0.20, 11.30 ± 0.37 and $13.08 \pm 0.34\%$ for the wild-type, Q31R, Q60R and F57L/Q60R HypF-N, respectively, (Fig. 4A, inset). Considering that the observed increases in total α-helical content are the result of marked local increases at mutated sites, the estimated increases at the sites of mutation(s), calculated according to equation (4), is therefore $+3.2 \pm 2.8\%$ (Q31R, first helix), $+8.0 \pm 2.1\%$ (Q60R, second helix) and $+26.1 \pm 4.4\%$ (F57L/Q60R, second helix), in good agreement with the predictions by AGADIR.

The intrinsic fluorescence emission spectra of the three mutants of HypF-N in their acid-unfolded state at pH 1.7 were significantly different from that of the wild-type protein in both the overall fluorescence intensity and λ_{max} values (Fig. 4B). The Q31R and Q60R mutants showed ∼10% decrease in total fluorescence intensity compared to wild-type protein. By contrast, the total fluorescence intensity of the F57L/Q60R mutant was found to be ∼16% higher to that of the wild-type protein. The λ_{max} values of all the mutant proteins are blue-shifted compared to that of the wild-type protein (Fig. 4B, inset). The Q31R and Q60R showed blue-shifts of *ca.* 2 nm, while the double mutant showed a blue shift of *ca.* 4 nm (Fig. 4B, inset). This indicates that the tryptophan residues are buried to a greater extent in the acid-unfolded mutants compared to the acid-unfolded state of wild-type protein. The degree of tryptophan burial appears to increase from the wild-type protein to the double F57L/Q60R mutant, following a trend similar to that observed for the increase of α-helical content.

ANS preferentially binds to solvent-accessible hydrophobic clusters in a protein, producing a marked increase in its fluorescence emission intensity and a large blue shift of its λ_{max} value, typically from 520 nm to 480 nm, when compared with free ANS in water (Semisotnov *et al.*, 1991). Changes in ANS fluorescence parameters can thus efficiently detect structural alterations of a protein following changes of solution conditions or mutation. Figure 4C shows the fluorescence emission spectra of ANS in the presence of the various HypF-N variants at pH 1.7 (the free ANS spectrum was subtracted from all spectra). The ANS fluorescence appears to be enhanced by 3-fold when the wild-type protein is present, 5-fold for the Q31R and Q60R mutants and 8-fold for the F57L/Q60R double mutant. For all the HypF-N variants, the λ_{max} is also blue-shifted from 520 nm (free ANS) to 485–490 nm. Precisely, the λ_{max} values for the wild-type, Q31R, Q60R and F57L/Q60R are 489.7 ± 2.1, 490.3 ± 2.4, 485.8 ± 1.6 and 486.6 ± 2.3, respectively (Fig. 4C, inset). The enhanced ANS fluorescence and further blue-shift of the λ_{max} value indicates an increase in hydrophobic surface area in the mutants relative to the wild-type protein. These data, together with the intrinsic fluorescence data suggest that the HypF-N mutants adopt, in their acid-unfolded state, a structural ensemble that contains a more consolidated, yet solvent-exposed, hydrophobic core than the wild-type protein.

The apparent hydrodynamic diameters of wild-type and mutant proteins in their acid-unfolded state at pH 1.7 were determined with DLS (Fig. 4D). These were found to be 5.7 ± 0.2, 5.5 ± 0.1, 5.5 ± 0.1 and 5.2 ± 0.2 nm for wild-type, Q31R, Q60R and F57L/Q60R HypF-N, respectively (Fig. 4D, inset). The result obtained for the wild-type protein is again in agreement with previously reported data

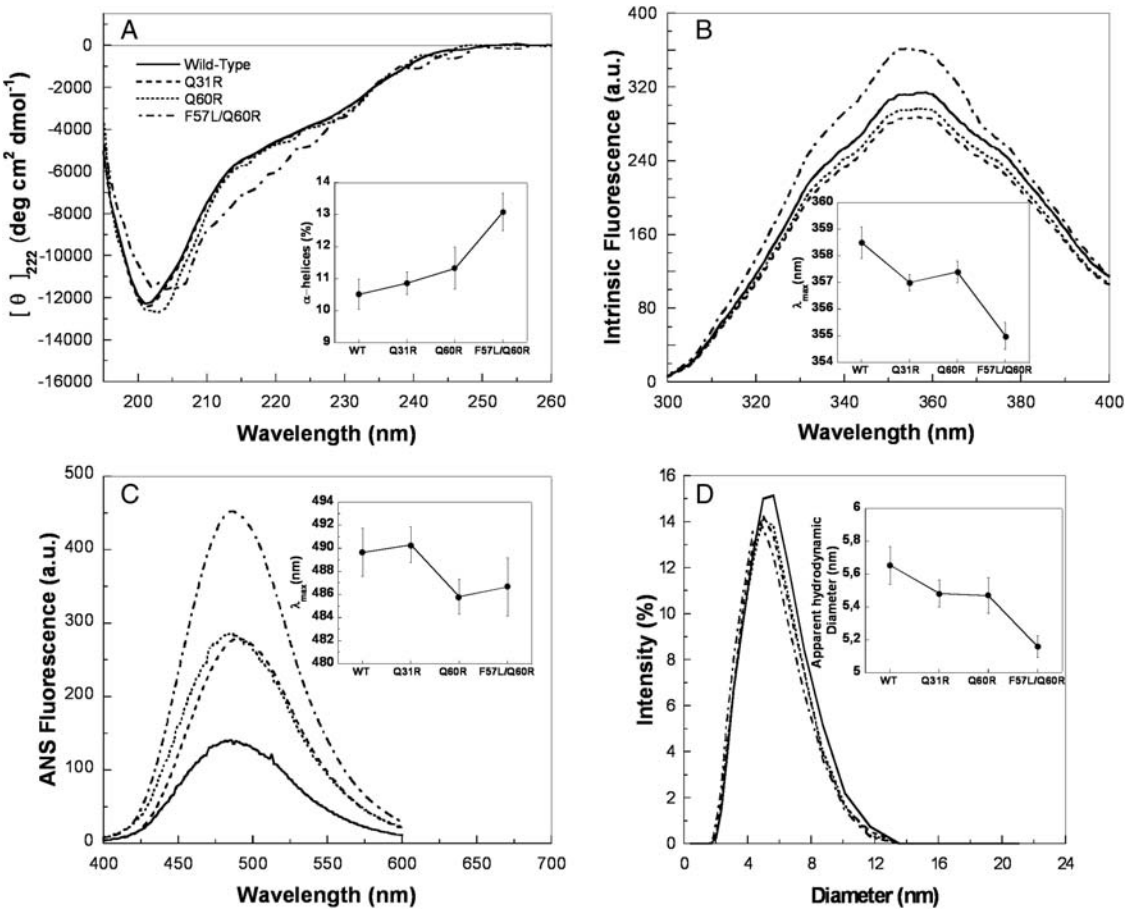

Fig. 4 Far-UV CD spectra (A), intrinsic fluorescence emission spectra (B), ANS fluorescence emission spectra (C) and size distributions obtained with DLS (D) for the HypF-N variants. The data refer to wild-type (—), Q31R (– –), Q60R (·····) and F57L/Q60R (–·–·–) HypF-N. All measurements were carried out in 20 mM TFA, 50 mM ionic strength, 2 mM DTT, pH 1.7, 25°C. In each panel the inset displays the values of a specific parameter, for the four analysed HypF-N variants extracted from the spectra shown in the corresponding main panel. In (A), inset, the numbers in brackets indicate the changes in α-helical content at the site of mutation relative to the wild-type sequence. Error bars indicate standard errors.

(Campioni *et al*., 2008). The increase in compactness observed with DLS for the acid-denatured HypF-N mutants at pH 1.7 is consistent with the increase of tertiary structure monitored by intrinsic and ANS-derived fluorescence.

Overall, following the analysis carried out with far-UV CD, intrinsic fluorescence, ANS fluorescence and DLS, the α-helical content of the acid-unfolded state of HypF-N appears to increase from the wild-type to the mutants at the corresponding sites of mutation(s), with such an increase correlating with burial of tryptophan residues, consolidation of the hydrophobic core and compactness. In this trend the F57L/Q60R double mutant features the most remarkable changes of all the measured parameters.

Conformational stability of HypF-N

We next investigated the conformational stabilities of the HypF-N variants by acquiring urea-induced unfolding curves at equilibrium at pH 7.0 and using far-UV CD as an optical probe to monitor unfolding. The aim of this analysis was not to evaluate the conformational stability of the native state for the 4 variants studied here, which is beyond the scope of the present work. It is rather to determine the cooperativity of the unfolding transition (i.e. the *m* values), which provides information on the differences of solvent-accessible surface area (ΔASA) on unfolding and, hence, on the compactness of the urea-unfolded state of the four analysed variants (Myers *et al*., 1995).

The urea-induced unfolding transitions of all the HypF-N variants at pH 7.0 were found to be single-step processes (Fig. 5A). The transitions were also found to be completely reversible for all the mutants. By fitting the experimental data to a two-state model (equation (2)) the values of ΔG^{H_2O}, *m* and midpoint of unfolding transition (C_m) were determined for all the studied HypF-N variants. The analysis yielded ΔG^{H_2O} and *m* values of 33.4 ± 3.4 kJ mol^{-1} and 7.3 ± 0.7 for wild-type HypF-N, which are in good agreement with those previously determined (Calloni *et al*., 2003, 2005). The midpoint of the unfolding transition of the mutants was not found to be higher than that of wild type. This was found to be 4.58 ± 0.06, 4.56 ± 0.08, 4.54 ± 0.07 and 4.42 ± 0.08 M for wild type, Q31R, Q60R and F57L/Q60R, respectively. The *m* values for the mutants were observed to be lower than that of the wild-type protein: 7.3 ± 0.3, 6.2 ± 0.2, 6.6 ± 0.2 and 6.2 ± 0.2 for wild type, Q31R, Q60R and F57L/Q60R, respectively (Fig. 5A, inset). On the other hand, the ΔG^{H_2O} values were calculated to be 33.4 ± 3.4, 28.3 ± 2.7, 29.9 ± 3.0 and 27.6 ± 3.8 kJ mol^{-1} for wild type, Q31R, Q60R and F57L/Q60R HypF-N, respectively. The decrease in ΔG^{H_2O} values for the mutants compared to the wild-type protein are due to the low *m*

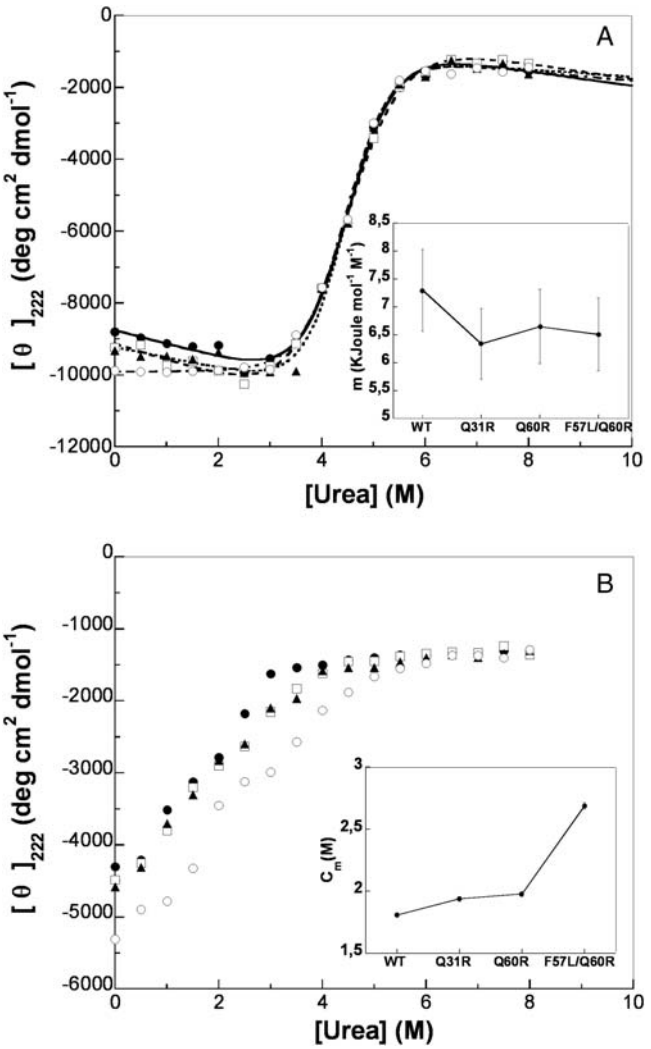

Fig. 5 Urea-induced unfolding at equilibrium of HypF-N variants in their native states at pH 7.0 (A) and acid-unfolded states at pH 1.7 (B), monitored by mean residue ellipticity at 222 nm. The lines through the data points were obtained by fitting the data to a two-state model (equation (2)). The data and the lines of best fit refer to WT (—•—), Q31R (–-□–-), Q60R (···▲···) and F57L/Q60R (–·–○–·–) HypF-N. The insets show the *m* values obtained at pH 7.0 (A) and the C_m values measured at pH 1.7 (B) of the HypF-N variants resulting from the procedure of best fitting.

values displayed by the mutants. The analysis therefore shows that the mutations result in an increased compactness of the urea-unfolded state.

We repeated the experiments at pH 1.7, thus under condition in which the four HypF-N variants populate initially, in the absence of urea, the acid-unfolded state. This set of experiments allowed the conformational stability of the acid-unfolded state to be evaluated for the four variants, particularly by determining the urea concentration at which the transition from the acid-unfolded state to the fully unfolded state in urea has occurred to 50%. All the mutants appeared to unfold in a non-cooperative manner (Fig. 5B). The mid-points of the transition for wild type, Q31R, Q60R and F57L/Q60R HypF-N were calculated to be 1.81 ± 0.08, 1.94 ± 0.06, 1.98 ± 0.15 and 2.69 ± 0.15 M, respectively (Fig. 5B, inset). Interestingly, the midpoint of the transition was found to correlate with the increase of α-helical content, consolidation of hydrophobic core and compactness in the acid-unfolded variants.

Kinetics of aggregation of HypF-N mutants

Wild-type HypF-N, at a protein concentration of 0.5 mg/ml (48 μM), was found to aggregate in 20 mM trifluoroacetic acid (TFA), 330 mM NaCl, 2 mM DTT, pH 1.7, 25°C (Campioni *et al.*, 2008). Aggregation was detected as an exponential increase in ThT fluorescence and as the formation of small spherical aggregates of 3–4 nm diameter, as detected with AFM (Campioni *et al.*, 2008; Calloni *et al.*, 2008). Such protein aggregates convert subsequently into protofibrils formed by the association of the beads after a few weeks (Campioni *et al.*, 2008).

In order to assess whether the increase of secondary and tertiary structure observed in the mutants causes a change in the aggregation rate, the aggregation kinetics of the HypF-N variants were monitored by ThT fluorescence under the aforementioned conditions. Figure 6 reports the time courses of ThT fluorescence for all the HypF-N variants, each analysed 3–4 times. The ThT traces were found to be reproducible for the same protein variant and were satisfactorily fitted to a single-exponential function (equation (5)). The resulting aggregation rate constant (k_{agg}) values show that the mutants aggregate with a rate similar to that of the wild-type protein (Fig. 6D, inset). The single and double mutants involving α-helix 2 (Q60R and F57L/Q60R) were found to aggregate with a rate slightly higher than the wild-type protein. However, the rates of the two mutants were similar and did not correlate with the difference of α-helical and tertiary structure observed between them with all structural probes. More generally, no correlation was observed between the k_{agg} values and the α-helical content, or tertiary structure content, in the protein variants analysed here.

We also analysed the morphologies of the aggregates formed after 2 h with AFM (Fig. 7). The oligomers formed by wild-type HypF-N appear to have spherical or discoid shape and to have a height of 2.8 ± 0.4 nm (Fig. 7A, F), in agreement with previous reports (Campioni *et al.*, 2008, 2010; Calloni *et al.*, 2008). The oligomers formed by the three mutants appear to be similar in size and height (Fig. 7B–D, F), indicating that the variants analysed here and the wild-type protein form the same type of oligomeric structures.

Discussion

α-Helical stability and aggregation rate are uncorrelated in highly dynamic states

HypF-N is a 91 residue, *α/β* protein belonging to the acylphosphatase-like structural family and having a ferredoxin-like fold with two α-helices packed against a five-stranded β-sheet (Rosano *et al.*, 2002). The formation of a partially folded state is a key event in the aggregation pathway of this protein *in vitro*, even under mild destabilising conditions in which the folded state is by far the predominant species (Chiti *et al.*, 2001; Marcon *et al.*, 2005). Under acidic conditions HypF-N unfolds into a partially folded state with all the characteristics of pre-molten globule state; such a conformational state was shown to be monomeric, possess a significant level of secondary structure and display the presence of a rudimental core, as revealed by far-UV CD, intrinsic fluorescence, ANS binding and DLS (Campioni *et al.*, 2008). NMR spectroscopy allowed one to

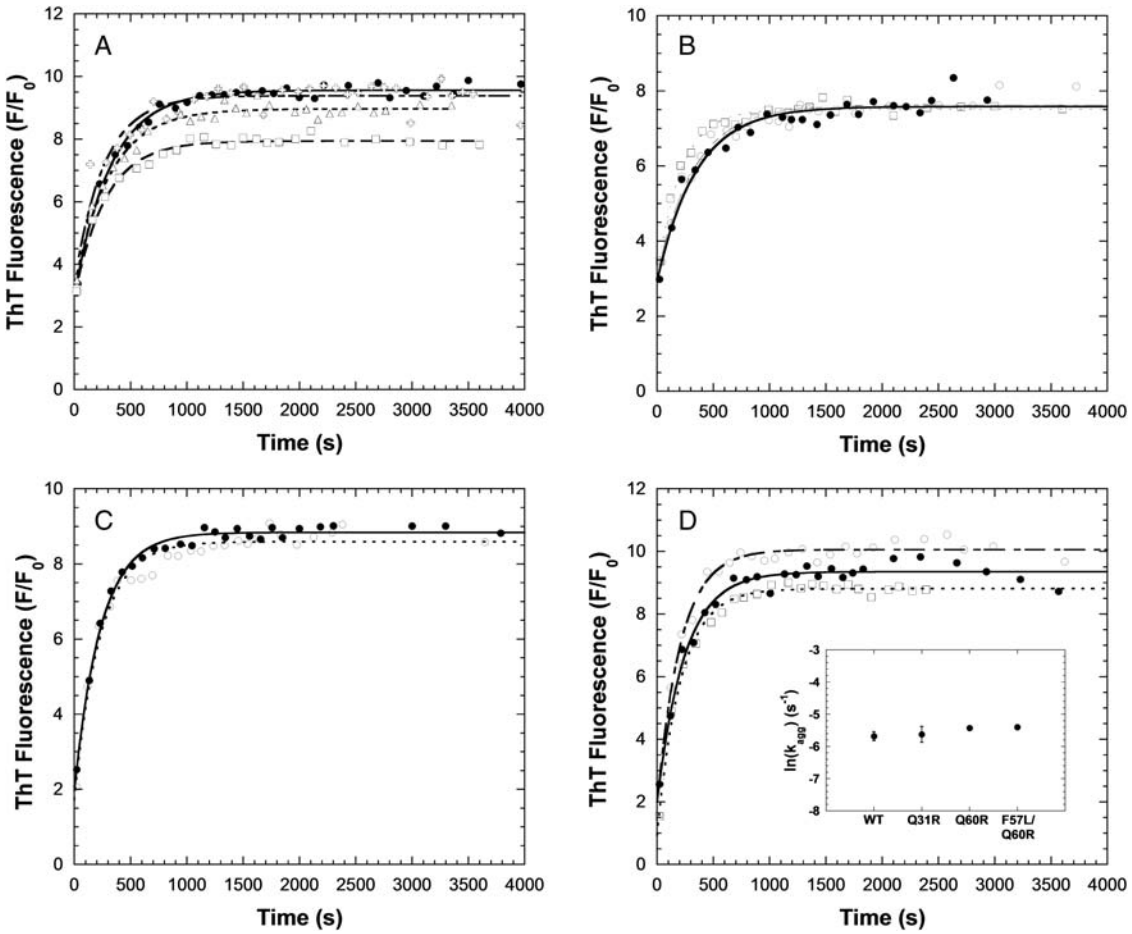

Fig. 6 Aggregation time courses of HypF-N variants, monitored with ThT fluorescence, in 20 mM TFA, 330 mM NaCl, 2 mM DTT, pH 1.7, 25°C. The traces refer to wild-type (A), Q31R (B), Q60R (C) and F57L/Q60R (D). Each panel reports multiple traces for the same protein variant, which are differentiated by symbol and line type. In all cases data are reported as the ratio of ThT fluorescence in the presence (F) and absence (F_0) of protein as a function of time. The lines of best fit through the data points were obtained by fitting the data with a single exponential function (equation (5)). The inset in (D) shows the aggregation rate constant (k_{agg}) values obtained from the procedure of best fitting for all HypF-N variants: the data and associated experimental errors are means and standard deviations, respectively.

identify the regions of the sequence that are most structured, albeit flexible, in the acid-denatured state (Calloni *et al.*, 2008). It was found that the regions of the sequence encompassing residues 23−34, 56−64 and 81−82, corresponding to the three major hydrophobic regions of the sequence, form interactions between them, although such interactions are flexible and in slow exchange (Calloni *et al.*, 2008). Moreover, the regions of sequence encompassing residues 26−30, 56−61 and 46−49 adopt a partially formed α-helical structure. Hence, it appears that the first two of such three regions, which also adopt α-helical structure in the native state, participate to the flexible hydrophobic core and adopt α-helical structure in the acid-denatured state of HypF-N.

The data presented in this paper show that the increase in α-helical propensity at the level of either α-helix in the acid-denatured state of HypF-N results in an increased amount of α-helical structure (Fig. 4A). Such an increase is small if calculated on the overall sequence, but is marked at the site(s) of mutation, amounting to $+26.1 \pm 4.4\%$ in the double mutant in a scale from 0% (no helix) to 100% (fully formed helix). The stabilisation of either α-helix also results in a consolidation of the hydrophobic core, as detected using intrinsic and ANS-derived fluorescence measurements (Fig. 4B, C), and in a compaction of the denatured ensemble, as indicated by DLS and measurements of the m value in urea-unfolding at equilibrium (Figs. 4D, 5A). Since the two regions of the sequence subjected to mutation in this study participate to both the α-helical structure and the formation of the rudimental hydrophobic core, it is likely that the consolidation of the amphipathic helices also brings a positive contribution to the consolidation of the hydrophobic core and the overall compactness of the acid-denatured state.

The acid-denatured state of wild-type HypF-N obtained at pH 1.7 was known to convert, at 350 mM ionic strength on the timescale of a few hours, into spherical oligomers with a height of ca. 3 nm, with a large amount of β-sheet structure and an ability to bind ThT (Campioni *et al.*, 2008, 2010; Calloni *et al.*, 2008). The mutants with stabilised α-helical structure used in this study were found to aggregate into similar spherical oligomers, as shown by AFM (Fig. 7), with a rate that did not appear to be significantly different from that of the wild-type protein, as shown by the ThT fluorescence time courses (Fig. 6). This indicates that the consolidation of α-helical structure in the acid-denatured state of HypF-N does not lead to a significant change of the

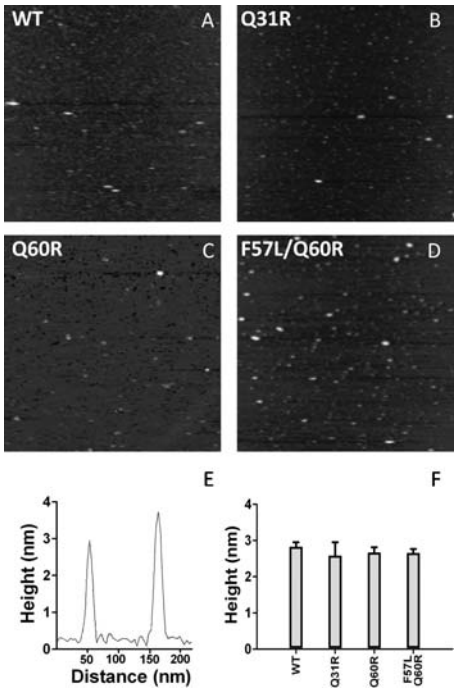

Fig. 7 AFM images of wild-type (A), Q31R (B), Q60R (C) and F57L/Q60R (D) HypF-N (scan size: 1 μm). All variants were pre-incubated for 2 h in 20 mM TFA, 330 mM NaCl, 2 mM DTT, pH 1.7, 25°C. (E) Example of a *Z* profile used to measure oligomer height. (F) Oligomer height (mean ± standard error) of wild-type ($n = 12$), Q31R ($n = 10$), Q60R ($n = 14$) and F57L/Q60R ($n = 17$) HypF-N.

aggregation rate of the protein from such a conformational state. This result is remarkable when considering that the two regions subjected to mutation not just retain α-helical structure in the acid-denatured state of HypF-N, but also are shown to be involved in the rate-determining steps of the conversion of this state into oligomers as well as in the structural core of the resulting aggregates (Calloni *et al.*, 2008; Campioni *et al.*, 2010).

Previous attempts to investigate the role of α-helical structure contained in unstructured states on amyloid formation have relied on the induction of α-helical structure by remarkable changes of solution conditions or by the introduction of non-conservative mutations. Both changes, however, also led to alterations of other variables that are known to play an important role in protein aggregation and cannot therefore represent valid perturbations to specifically investigate the role of α-helical structure (see the Introduction section). In this study protein engineering has been carried out to target only the propensity of forming α-helical structure: we have further increased the α-helical propensity of partially formed α-helices while maintaining the same solution conditions and minimising the alterations of the physicochemical, sequence-specific parameters involved in protein aggregation (Fig. 2).

In our previous study it was shown that the regions of the HypF-N sequence that promote the conversion of the acid-denatured state into ThT-binding and β-sheet containing oligomers coincide with the peaks of the aggregation propensity profile, meaning that they have the sequence-based physicochemical parameters appropriate for triggering amyloid formation (Calloni *et al.*, 2008). No correlation was found between such stretches and those forming (or non-forming) secondary or tertiary structure in the acid-denatured state (Calloni *et al.*, 2008). The absence of a significant effect of the stability of α-helical structure on the aggregation of acid-denatured HypF-N reinforces the idea that the aggregation of highly dynamic conformational states into amyloid is not determined significantly by the non-persistent residual structure present in the initial monomeric state, but by amyloidogenic segments of the sequence that have a sufficiently high intrinsic aggregation propensity, which is determined on the basis of parameters such as hydrophobicity, β-sheet propensity and charge.

The importance of the stability and location of α-helical structure

A similar study was performed on the TFE-denatured state of human muscle acylphosphatase (mAcP); similarly to the case presented here, the α-helical propensity was increased in both regions adopting α-helical structure in the native state using mutations that did not alter significantly the intrinsic aggregation propensity (Taddei *et al.*, 2001). The mutations increasing the α-helical propensity of the first helix, which is also involved in aggregation, led to a significant deceleration of the aggregation process. The subject of that study was, however, a TFE-denatured state, where the two α-helices were stabilised to a level similar to, or even more than, the native state. In other studies it was noticed that an excessive content of lipid membranes induces an over-stabilisation of the α-helical structure of IAPP, causing a substantial inhibition of amyloid formation by this peptide (Jayasinghe and Langen, 2005; Apostolidou *et al.*, 2008). Along the same lines, it has been found that one of the strategies used by evolution to neutralise amyloidogenic stretches within normally folded proteins is to hide them into α-helical segments (Tzotzos and Doig, 2010; Kallberg *et al.*, 2001). A distinction has to be made, therefore, between stable (persistently formed) and dynamic, partially formed (non-persistently formed) α-helical structures. The amyloidogenic potential of a sequence segment with a high intrinsic aggregation propensity can be decreased dramatically by adopting a stable α-helical structure, because the α-helical structure has to be unfolded to initiate aggregation. Strategies aimed at stabilising the helix further are likely to be effective in inhibiting aggregation in this case. On the other hand, unstable and partially formed helices are unlikely to represent an effective defence against the aggregation because the helix exposes its residues regularly during the structural fluctuations revealing the aggregation potential of its sequence. Increasing the α-helical propensity of such stretches does not inhibit aggregation in this case, unless the increase in α-helical propensity allows the helix to pass from the first to the second regime.

In other studies it has been proposed that the formation of amphipathic α-helices in initially disordered peptides can be a productive event for aggregation, provided the newly formed α-helices involve regions of the sequence that are not amyloidogenic (Abedini and Raleigh, 2009). Under these circumstances, the newly formed α-helices from different peptide molecules can form interactions via their hydrophobic surfaces, thus giving rise to oligomers where the unstructured amyloidogenic sequences are spatially closer. In such an oligomer the unstructured amyloidogenic stretches have an increased frequency of collisions, resulting into an acceleration of the formation of the cross-β structure motif

of amyloid (Abedini and Raleigh, 2009). In the study presented here, the stabilised α-helical structure involves regions of the sequence that are also amyloidogenic, thus representing a scenario distinct from that proposed previously for IAPP.

As a conclusion of our and other studies it appears that stabilisation of α-helical structure can cause an acceleration of the aggregation process depending on the initial stability and location of the α-helices. In particular the effect can vary if the stabilised helices are (i) in non-amyloidogenic stretches of initially unstructured peptides (accelerating effect), (ii) in amyloidogenic stretches of initially unstructured peptides (no effect) or (iii) in amyloidogenic stretches of initially stable helices (decelerating effect).

Acknowledgements

We thank Sandra Niccoli for assistance in atomic force microscopy.

Funding

This research was funded by the Ministero dell'Istruzione, Ricerca e Università (Projects FIRB RBNE03PX83 and PRIN 20083ERXWS) and the European Union (project EURAMY). The funders had no role in study design, data collection and analysis, decision to publish, preparation of the manuscript.

References

Abedini,A. and Raleigh,D.P. (2005) *Biochemistry*, **44**, 16284–16291.
Abedini,A. and Raleigh,D.P. (2009) *Protein Eng. Des. Sel.*, **22**, 453–459.
Apostolidou,M., Jayasinghe,S.A. and Langen,R. (2008) *J. Biol. Chem.*, **283**, 17205–17210.
Calloni,G., Taddei,N., Plaxco,K.W., Ramponi,G., Stefani,M. and Chiti,F. (2003) *J. Mol. Biol.*, **330**, 577–591.
Calloni,G., Zoffoli,S., Stefani,M., Dobson,C.M. and Chiti,F. (2005) *J. Biol. Chem.*, **280**, 10607–10613.
Calloni,G., Lendel,C., Campioni,S., Giannini,S., Gliozzi,A., Relini,A., Vendruscolo,M., Dobson,C.M., Salvatella,X. and Chiti,F. (2008) *J. Am. Chem. Soc.*, **130**, 13040–13050.
Campioni,S., Mossuto,M.F., Torrassa,S., Calloni,G., de Laureto,P.P., Relini,A., Fontana,A. and Chiti,F. (2008) *J. Mol. Biol.*, **379**, 554–567.
Campioni,S., Mannini,B., Zampagni,M., *et al*. (2010) *Nat. Chem. Biol.*, **6**, 140–147.
Chiti,F. and Dobson,C.M. (2006) *Annu. Rev. Biochem.*, **75**, 333–366.
Chiti,F. and Dobson,C.M. (2009) *Nat. Chem. Biol.*, **5**, 15–22.
Chiti,F., Bucciantini,M., Capanni,C., Taddei,N., Dobson,C.M. and Stefani,M. (2001) *Protein Sci.*, **10**, 2541–2547.
Chiti,F., Stefani,M., Taddei,N., Ramponi,G. and Dobson,C.M. (2003) *Nature*, **424**, 805–808.
Conchillo-Solé,O., de Groot,N.S., Avilés,F.X., Vendrell,J., Daura,X. and Ventura,S. (2007) *BMC Bioinformatics*, **8**, 65.
Dobson,C.M. (1999) *Trends Biochem. Sci.*, **24**, 329–332.
Fernandez-Escamilla,A.M., Rousseau,F., Schymkowitz,J. and Serrano,L. (2004) *Nat. Biotechnol.*, **22**, 1302–1306.
Fezoui,Y. and Teplow,D.B. (2002) *J. Biol. Chem.*, **277**, 36948–36954.
Galzitskaya,O.V., Garbuzynskiy,S.O. and Lobanov,M.Y. (2006) *PLoS Comput. Biol.*, **2**, e177.
Jahn,T.R. and Radford,S.E. (2008) *Arch. Biochem. Biophys.*, **469**, 100–117.
Jayasinghe,S.A. and Langen,R. (2005) *Biochemistry*, **44**, 12113–12119.
Kallberg,Y., Gustafsson,M., Persson,B., Thyberg,J. and Johansson,J. (2001) *J. Biol. Chem.*, **276**, 12945–12950.
Kirkitadze,M.D., Condron,M.M. and Teplow,D.B. (2001) *J. Mol. Biol.*, **312**, 1103–1119.
Knight,J.D., Hebda,J.A. and Miranker,A.D. (2006) *Biochemistry*, **45**, 9496–9508.
Ling,Y.L., Strasfeld,D.B., Shim,S.H., Raleigh,D.P. and Zanni,M.T. (2009) *J. Phys. Chem. B.*, **113**, 2498–2505.
Marcon,G., Plakoutsi,G., Canale,C., Relini,A., Taddei,N., Dobson,C.M., Ramponi,G. and Chiti,F. (2005) *J. Mol. Biol.*, **347**, 323–335.
Maurer-Stroh,S., Debulpaep,M., Kuemmerer,N., *et al*. (2010) *Nat. Methods*, **7**, 237–242.
Monsellier,E. and Chiti,F. (2007) *EMBO Rep.*, **8**, 737–742.
Morrow,J.A., Segal,M.L., Lund-Katz,S., Philips,M.C., Knapp,M.B., Rupp and Weigraber,K.H. (2002) *Biochemistry*, **39**, 11657–11666.
Muñoz,V. and Serrano,L. (1994) *Nat. Struct. Biol.*, **1**, 399–409.
Myers,J.K., Pace,C.N. and Scholtz,J.M. (1995) *Protein Sci.*, **4**, 2138–2148.
Padrick,S.B. and Miranker,A.D. (2002) *Biochemistry*, **41**, 4694–4703.
Päiviö,A., Nordling,E., Kallberg,Y., Thyberg,J. and Johansson,J. (2004) *Protein Sci.*, **13**, 1251–1259.
Pawar,A.P., Dubay,K.F., Zurdo,J., Chiti,F., Vendruscolo,M. and Dobson,C.M. (2005) *J. Mol. Biol.*, **350**, 379–392.
Relini,A., Torrassa,S., Rolandi,R., *et al*. (2004) *J. Mol. Biol.*, **338**, 943–957.
Rosano,C., Zuccotti,S., Bucciantini,M., Stefani,M., Ramponi,G. and Bolognesi,M. (2002) *J. Mol. Biol.*, **321**, 785–796.
Santoro,M.M. and Bolen,D.W. (1988) *Biochemistry*, **27**, 8063–8068.
Semisotnov,G.V., Rodionova,N.A., Razgulyaev,O.I., Uversky,V.N., Gripas,A.F. and Gilmanshin,R.I. (1991) *Biopolymers*, **31**, 119–128.
Stefani,M. and Dobson,C.M. (2003) *J. Mol. Med.*, **81**, 678–699.
Taddei,N., Capanni,C., Chiti,F., Stefani,M., Dobson,C.M. and Ramponi,G. (2001) *J. Biol. Chem.*, **276**, 37149–37154.
Tartaglia,G.G., Pawar,A., Campioni,S., Chiti,F., Dobson,C.M. and Vendruscolo,M. (2008) *J. Mol. Biol.*, **380**, 425–436.
Tartaglia,G.G., Cavalli,A., Pellarin,R. and Caflisch,A. (2005) *Protein Sci.*, **14**, 2723–2734.
Trovato,A., Chiti,F., Maritan,A. and Seno,F. (2006) *PLoS Comput. Biol.*, **2**, e170.
Tzotzos,S. and Doig,A.J. (2010) *Protein Sci.*, **19**, 327–348.
Uversky,V.N. and Fink,A.L. (2004) *Biochim. Biophys. Acta*, **1698**, 131–153.
Ventura,S. and Villaverde,A. (2006). *Trends Biotechnol.*, **24**, 179–185.
Villegas,V., Zurdo,J., Filimonov,V.V., Avilés,F.X., Dobson,C.M. and Serrano,L. (2000) *Protein Sci.*, **9**, 1700–1708.
Yoon,S. and Welsh,W.J. (2004) *Protein Sci.*, **13**, 2149–2160.